NANOMATERIALS

Building superlattices from individual nanoparticles via template-confined DNA-mediated assembly

Qing-Yuan Lin,[1,3]* Jarad A. Mason,[1,2]* Zhongyang Li,[4]* Wenjie Zhou,[1,2] Matthew N. O'Brien,[1,2] Keith A. Brown,[1,2] Matthew R. Jones,[1,3] Serkan Butun,[4] Byeongdu Lee,[5] Vinayak P. Dravid,[1,3]† Koray Aydin,[4]† Chad A. Mirkin[1,2,3]†

DNA programmable assembly has been combined with top-down lithography to construct superlattices of discrete, reconfigurable nanoparticle architectures on a gold surface over large areas. Specifically, the assembly of individual colloidal plasmonic nanoparticles with different shapes and sizes is controlled by oligonucleotides containing "locked" nucleic acids and confined environments provided by polymer pores to yield oriented architectures that feature tunable arrangements and independently controllable distances at both nanometer- and micrometer-length scales. These structures, which would be difficult to construct by other common assembly methods, provide a platform to systematically study and control light-matter interactions in nanoparticle-based optical materials. The generality and potential of this approach are explored by identifying a broadband absorber with a solvent polarity response that allows dynamic tuning of visible light absorption.

DNA has become a powerful tool for constructing highly ordered materials from nanoparticle (NP) building blocks (*1*–*3*). Indeed, the tunability afforded by the sequence-specific interactions inherent to oligonucleotides has been leveraged to assemble NPs into many exotic structures, including colloidal crystals that feature more than 30 different lattice symmetries, tunable interparticle distances ranging from below 3 nm to above 130 nm, and multiple well-defined crystal habits (*4*–*7*). In contrast to the diversity of structures that have been synthesized in solution, DNA has only been used to generate a relatively limited set of NP structures on surfaces (*8*–*10*). Moreover, the use of DNA—as well as any other bottom-up or combination of bottom-up and top-down assembly techniques—to transfer colloidal NPs from solution to a surface has led to either NP monolayers or three-dimensional (3D) extended lattices (*11*–*14*), whereas the synthesis of isolated nanostructures that incorporate multiple NP sizes, shapes, and/or compositions has remained elusive. The ability to predictably, rapidly, and precisely place individual NPs into desired arrangements—regardless of size, shape, or composition—over large areas on a surface in both two and three dimensions would represent a considerable advance in structural control, dramatically expanding the range of nanomaterials that can be synthesized and enabling new properties, many of which have likely never even been contemplated because of a lack of access to such structures.

With most assembly techniques, it is extremely challenging to control the thermodynamics of interactions both between NPs and between NPs and a surface, as would be required to build discrete, surface-bound architectures with a high level of structural control. Here, by using DNA programmable interactions to direct the layer-by-layer assembly of colloidal NPs within a polymer template, we realize oriented superlattices of multicomponent NP architectures. Confined environments provided by the pores of the polymer template enable the construction of architectures perpendicular to the substrate, whereas precisely engineered NP-NP interactions mediated by DNA allow architectures to be assembled a single NP at a time with controlled interparticle distances. These NP superlattices can be specified and independently controlled by the 2D template and the 1D arrangement of the oriented, NP architecture. Because of the oligonucleotide bonding elements that hold them in place, these architectures undergo reversible structural changes in response to chemical stimuli, allowing interactions with visible light to be dynamically tuned.

To arrange colloidal NPs into desired architectures on a surface (Fig. 1), we used electron-beam lithography (EBL) to pattern a uniform array of pores into a 300-nm-thick layer of poly(methyl methacrylate) (PMMA) affixed to a gold-coated silicon substrate (*9*). The selectively exposed gold surfaces at the bottom of each pore were then densely functionalized with oligonucleotides bearing a terminal propylthiol [DNA sequences are provided in table S1 (*15*)]. Complementary oligonucleotides were then hybridized to the single-stranded DNA at the base of each pore to yield a monolayer of rigid, double-stranded DNA with a short single-stranded region, or "sticky end," at the solution-facing terminus.

Colloidal gold NPs of different shapes and sizes (fig. S1) were similarly modified with DNA. Architectures of DNA-functionalized NPs were then assembled within each pore of the PMMA template in a layer-by-layer manner by designing the sticky-end DNA sequence present on a selected NP to be complementary to that of the previous layer (Fig. 1). To achieve a predictable, thermodynamically favored arrangement of NPs in each layer, the assembly process must be governed by the maximization of canonical Watson-Crick DNA hybridization events between complementary DNA sticky ends—a principle known as the complementary contact model (*3*, *16*). For this interaction to dominate, we needed to mitigate the effects of other nonspecific interactions that compete at low temperatures, such as interactions between noncomplementary nucleic acids and between DNA and the PMMA template.

Anisotropic NPs with flat facets and adenine- or guanine-containing sticky ends are particularly prone to a range of noncanonical interactions (*8*, *17*). The impact of these interactions can be reduced by performing the assembly at higher temperatures, but high temperatures may also lead to the dehybridization and desorption of NP layers that have already been assembled (fig. S2) (*8*). Indeed, finding a suitable assembly temperature for the synthesis of architectures in both high yield and high purity proved to be challenging when sticky ends were composed of conventional nucleic acids (fig. S3A).

To increase the strength of Watson-Crick DNA hybridization interactions between sticky ends relative to noncanonical ones, we replaced three adenine nucleotides in sticky-end sequences with "locked" versions containing the same base (table S1). Locked nucleic acids (LNA) are modified RNA nucleotides in which the ribose group is rigidified by connecting the 2′ oxygen to the 4′ carbon with a methylene bridge (*18*, *19*). This modification reduces conformational flexibility and increases the strength of canonical base-pairing interactions. Incorporating just three LNA bases into the sticky-end sequences of nanocubes increased the melting temperature associated with canonical hybridization interactions by 9°C, while also decreasing the melting temperature for noncanonical interactions by 1°C (fig. S3B). This 10°C greater window for NP assembly enabled the predictable synthesis of highly uniform superlattices composed of one-, two-, and three-layer NP architectures.

In addition to DNA, the size, shape, depth, and arrangement of PMMA pores provide a critical element of structural control during NP assembly [additional discussion of the relationships between pore design and NP assembly is provided in the supplementary text (*15*)]. For example, the depth of each pore, which was determined by the

[1]International Institute for Nanotechnology, Northwestern University, Evanston, IL 60208, USA. [2]Department of Chemistry, Northwestern University, Evanston, IL 60208, USA. [3]Department of Materials Science and Engineering, Northwestern University, Evanston, IL 60208, USA. [4]Department of Electrical Engineering and Computer Science, Northwestern University, Evanston, IL 60208, USA. [5]X-ray Science Division, Argonne National Laboratory, 9700 South Cass Avenue, Argonne, IL 60439, USA.
*These authors contributed equally to this work.
†Corresponding author. Email: chadnano@northwestern.edu (C.A.M.); aydin@northwestern.edu (K.A.); v-dravid@northwestern.edu (V.P.D.)

thickness of PMMA, provided a confined environment for the assembly of each NP layer. We could then build 1D architectures a single NP at a time exclusively in a direction perpendicular to the substrate. Additionally, NPs would not assemble in a pore smaller than the NP, whereas multiple NPs would assemble in larger pores (figs. S4 and S5). Choosing a pore size slightly larger than the total size of the NP and DNA thus allowed us to assemble uniform monolayers of different size and shape NPs into arrays (Fig. 2) (*9*). The pore shape further offers the ability to align the average orientation of anisotropic NPs, as observed for cubes assembled in square pores and triangular prisms assembled in triangular pores (Fig. 2, B and C, and fig. S37). After assembly, the porous PMMA template could be dissolved and the NP superlattices transferred intact to the solid state for imaging by scanning electron microscopy (SEM) (Fig. 1 and fig. S7).

In addition to monolayers of isolated NPs, we used template-confined, DNA-mediated assembly to synthesize superlattices with 2D periodicity featuring 10 different unit cells that each consist of a 1D architecture of either two or three NPs oriented normal to the surface (Fig. 3A and figs. S8 to S17). These 1D architectures include building blocks of the same size and shape, building blocks of decreasing size, and building blocks of different sizes and shapes. Superlattices of these low-symmetry architectures were synthesized over areas of at least 600 by 600 μm with high uniformity (Fig. 3, B and D, and fig. S18). Grazing-incidence small-angle x-ray scattering (GISAXS) confirmed that the superlattices exhibited the expected diffraction patterns—lines in reciprocal space—of a material with 2D periodicity (Fig. 3C and fig. S19). This bottom-up, layer-by-layer assembly process overcame several challenges in the fabrication of multilayer architectures with conventional top-down techniques, such as focused ion beam (FIB) milling (*20*) or EBL stacking (*21*), which require time-consuming, small-scale cutting of materials or complex serial alignment, exposure, development, and metal evaporation to form each layer. Here, biomolecular interactions operating at molecular-length scales allow for the rapid, automatic, and precise alignment of each NP layer with tunable interlayer distances (fig. S21).

Not surprisingly, these NP superlattices contained several types of defects analogous to thermodynamically inevitable defects in atomic crystals, including "vacancies," where a NP was missing from a superlattice position, and "interstitials," where an extra NP was present within the superlattice (*22*). Each individual architecture within the superlattice could be resolved by electron microscopy, so these NP defects can be rigorously quantified and used to establish structure-property relations. For example, a representative disk-cube-sphere three-layer superlattice of 773 architectures contained 73% defect-free structures, 1% vacancies, 9% interstitials, and 17% other defects (Fig. 3D). In general, the number of defects tended to increase as the number of potential competing interactions increased in

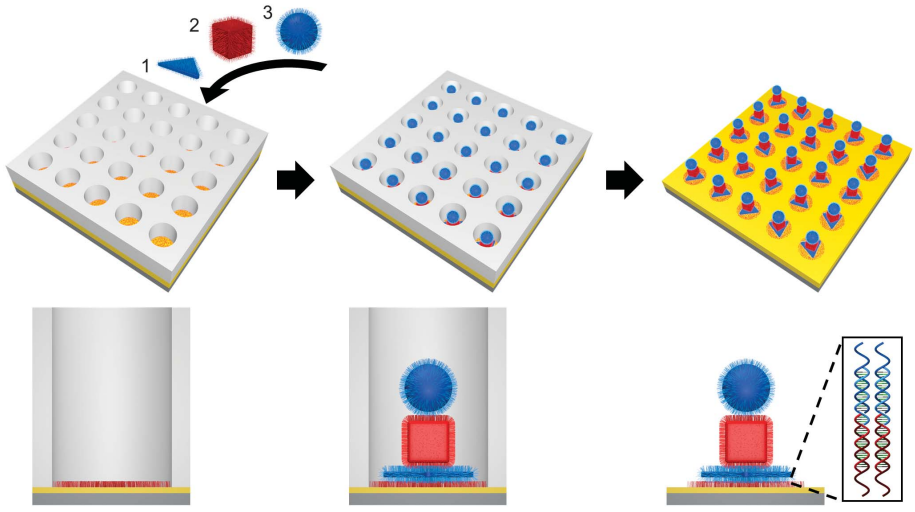

Fig. 1. Programmable assembly of reconfigurable nanoparticle (NP) architectures. To assemble NP architectures within a confined environment, 1D pores are fabricated in a PMMA-coated gold substrate using top-down lithography, and the gold surface at the bottom of each pore is densely functionalized with DNA. DNA-functionalized colloidal NPs of controlled size and shape are then assembled in a layer-by-layer manner by designing each layer of NPs to have a terminal DNA sequence complementary to that of the previous layer. The porous PMMA template is removed to generate NP superlattices with 2D periodicity that are composed of oriented NP architectures. Bottom images depict cross-sectional views of a single pore.

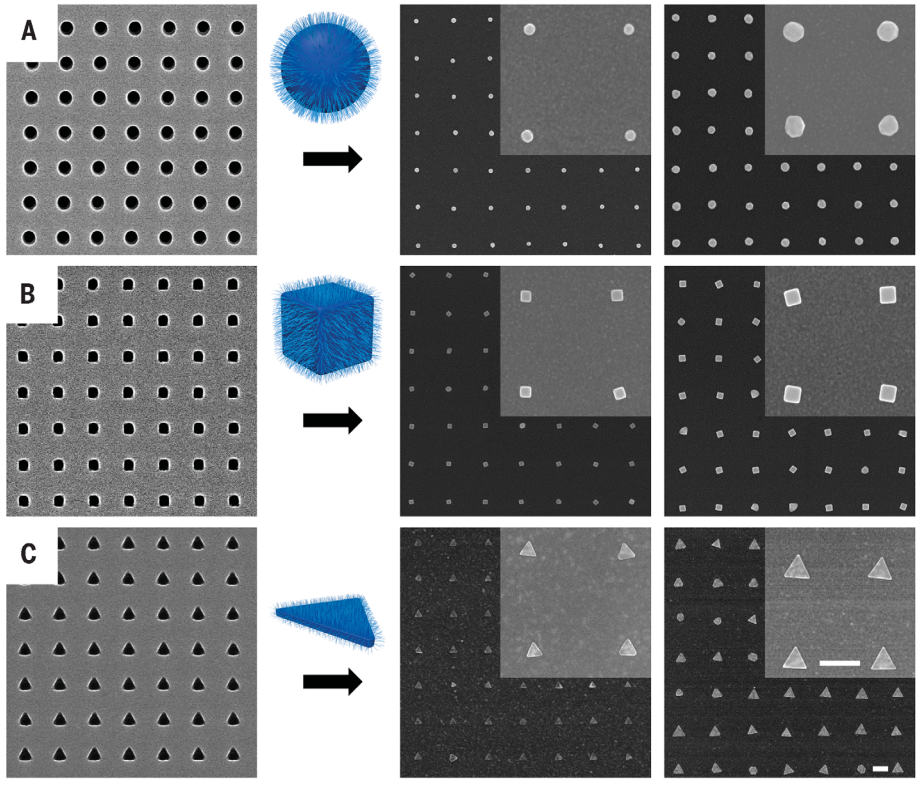

Fig. 2. Monolayer of DNA-functionalized gold NPs assembled in PMMA templates with different-shaped pores. (**A**) Circular pores (left) are used to assemble a monolayer of gold spheres 60 and 100 nm in diameter (right). (**B**) Square pores (left) are used to assemble a monolayer of gold cubes 55 and 80 nm in edge length (right). (**C**) Triangular pores (left) are used to assemble a monolayer of gold triangular prisms 90 and 165 nm in edge length (right). All SEM images of assembled nanoparticles are shown after the removal of the PMMA template. Scale bars, 200 nm.

moving from one- to two- to three-layer structures (figs. S8 to S17). However, the SEM images depict snapshots of the structures in the perturbed solid state, a consequence of drying, and the solution-based architectures likely exhibit greater uniformity.

In addition to directing NP assembly, oligonucleotide bonds between NPs are dynamic and undergo reversible contractions and expansions in response to changes in solvent polarity that allow the distance between NPs to be precisely tuned (*23*). Although it is a challenge to accurately measure the distance between NPs of different sizes and shapes in isolated architectures, cross-sectional SEM images of disk-cube-sphere architectures, which were encased in silica to attempt to preserve their solution-phase arrangements (*23*), showed that the average distance between NPs decreased from >12 nm to <3 nm when the solvent composition was adjusted from 0 to 80% ethanol (EtOH) in H_2O by volume at constant 0.3 M NaCl (Fig. 4D and fig. S20).

The synthesis of plasmonic NP architectures with structures and stimuli-responsive behavior that are not accessible in lithographically defined plasmonic nanostructures (*24*–*26*) provides an opportunity to design materials with emergent optical properties that offer new fundamental insights and previously inaccessible functionalities. As a proof-of-concept demonstration of the potential of our approach, we leveraged the tunability of oligonucleotide bonds to dynamically control light-matter interactions, enabling the exploration of active and reconfigurable plasmonic devices (*27*). Specifically, because the interparticle distances in the DNA-assembled NP superlattices reported here are within a region that should give rise to strong plasmonic coupling, we anticipated that even small changes to the arrangement of and spacing between coupled plasmonic NPs would lead to substantial changes in the absorption spectrum (*24*, *27*–*29*). It is not readily apparent, however, which NP architectures might offer the largest optical tuning range for a given change in the spacing between NPs.

To predict the effects of structural changes on interactions of light with plasmonic NP superlattices, finite-difference time-domain (FDTD) simulations were performed for multilayer superlattices with different periodicities, NP sizes and shapes, and gap distances, enabling us to screen for absorbers that feature large-magnitude wavelength and amplitude tunabilities (figs. S22 to S25). Based on these simulations, we identified a tunable broadband absorber in the visible regime—not yet realized experimentally and difficult to envision making by conventional lithography or assembly—composed of the following NP architectures: a sphere (60 nm in diameter) placed on top of a cube (76 nm in edge length) placed on top of a circular disk (105 nm in diameter, 7.5 nm in thickness) and arranged into square arrays with 200-nm periodicity on a 100-nm-thick gold substrate (Fig. 4A). FDTD simulations suggested that decreasing gap lengths from 16 to 4 nm within each NP architecture would increase the localized electric field intensity within the nanocavities at larger wavelengths (>690 nm), affording both very large wavelength tunability and amplitude modulation (Fig. 4, B and C, and fig. S26).

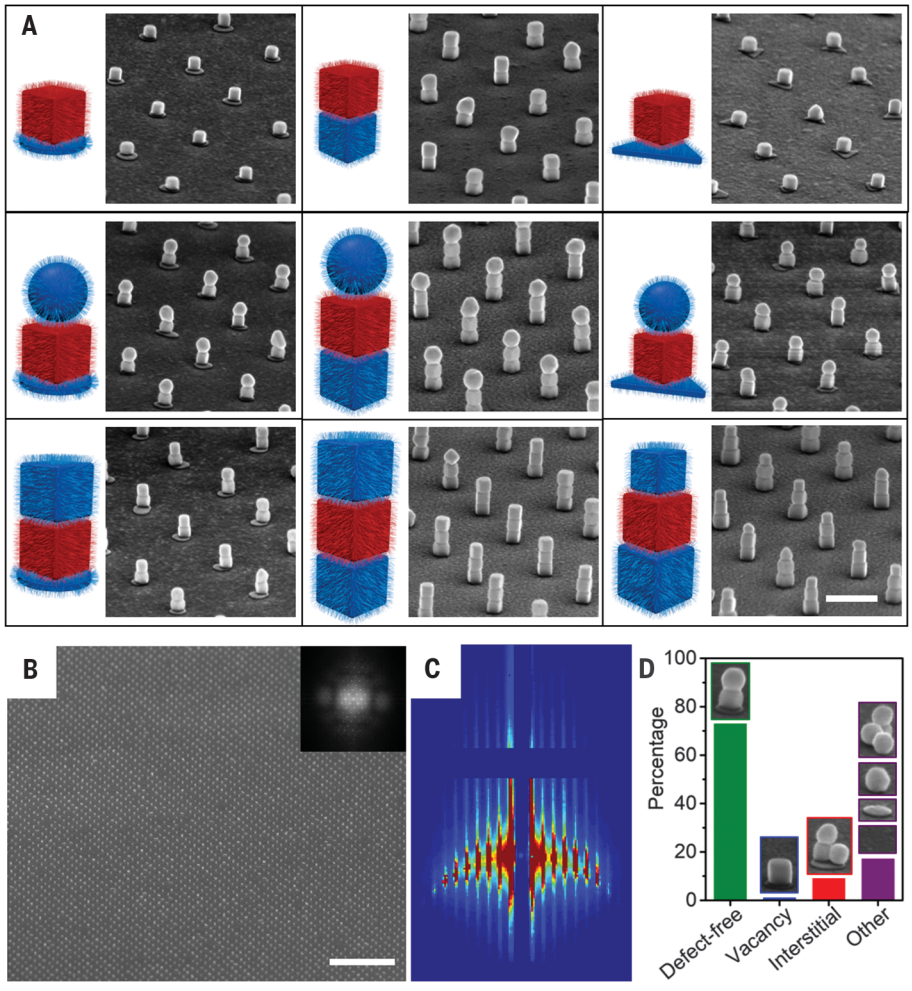

Fig. 3. Synthesis of oriented superlattices of two- and three-layer NP architectures. (**A**) SEM images of oriented superlattices (periodicity = 500 nm) attached to a gold surface after removal of the PMMA template. The superlattices are composed of 1D architectures of gold NPs in the order of: disk-cube, cube-cube, prism-cube, disk-cube-sphere, cube-cube-sphere, prism-cube-sphere, disk-cube-cube, cube-cube-cube (same size), and cube-cube-cube (decreasing sizes). Scale bar, 300 nm. (**B**) Large-area SEM image of the disk-cube-sphere superlattice. (Inset) Fast Fourier transform pattern of the SEM image. Scale bar, 4 μm. (**C**) GISAXS pattern of the disk-cube-sphere superlattice. (**D**) Defects in the disk-cube-sphere superlattice were quantified through analysis of SEM images that contained 773 individual unit cells within the superlattice.

To experimentally confirm the predicted optical response, the computationally identified NP superlattice—composed of discrete disk-cube-sphere architectures—was synthesized (fig. S27). Absorption spectra were measured with an inverted optical microscope for the superlattice coated with a thin layer of solvent with increasing ratios of EtOH to H_2O (Fig. 4E). As predicted, changing the average coupling distance between NPs led to dramatic changes in the absorption spectra, which are in excellent agreement with simulations—indicating that any defects or inhomogeneities present in the assembled superlattice do not considerably affect its optical properties—and confirmed the high tunability of this reconfigurable absorber (Fig. 4, E and F). Specifically, the superlattice had a 75% increase in the average absorption of light from 550 to 800 nm when decreasing solvent polarity—and decreasing average gap lengths—from 0 to 80% EtOH in H_2O, with a maximum increase of 443% at 732 nm (increased absorption from 14 to 73%). As expected, the changes in optical response could also be observed visually as the color of the surface changed from maroon to dark green to brown as gap lengths decreased (Fig. 4G).

In addition to the amplitude, the absorption band edge λ_{edge} could be tuned from 650 nm (1.9 eV) to 775 nm (1.6 eV) (Fig. 4, E and F). The 125-nm shift in wavelength represents a wavelength tuning figure of merit (wavelength shift divided

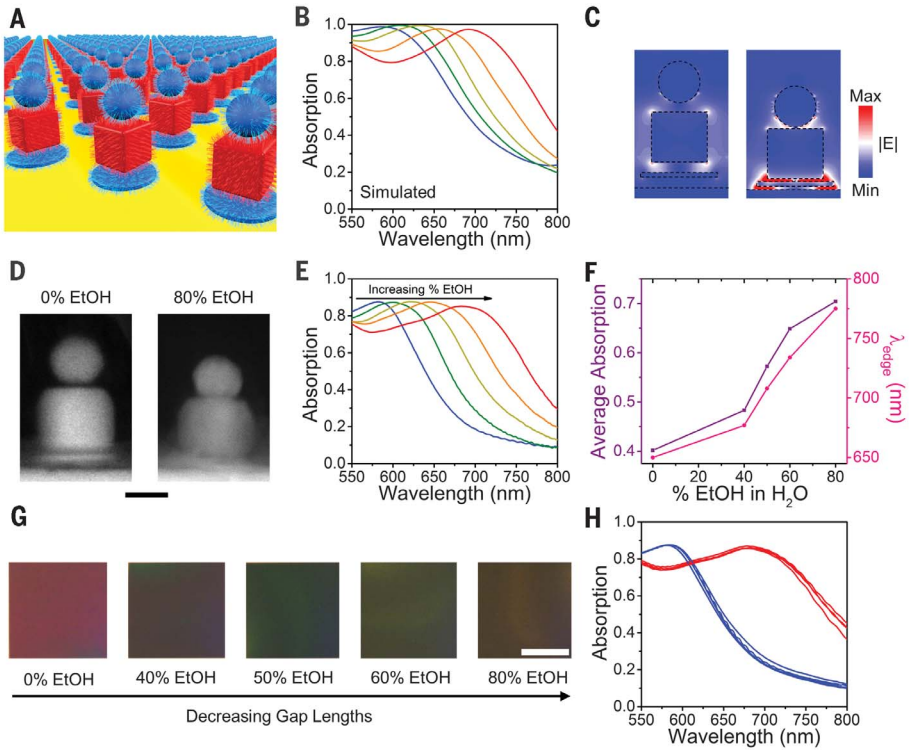

Fig. 4. Reconfigurable optical properties. (**A**) Each unit cell of the NP superlattice consists of a gold surface, circular disk, cube, and sphere, with experimentally matched dimensions. (**B**) FDTD simulations of optical absorption spectra of the disk-cube-sphere superlattice with 16-, 10-, 8-, 6-, and 4-nm gap lengths (from blue to red). (**C**) FDTD simulations of electric field distributions, $|E|$, for 16-nm gaps (left) and 4-nm gaps (right) at λ = 690 nm. (**D**) Cross-sectional SEM images of a single disk-cube-sphere architecture after immersing in 0% (left) and 80% (right) EtOH in H_2O at 0.3 M NaCl. Superlattices were encased in silica before imaging to preserve the solution-phase structure in the solid state. Scale bar, 50 nm. (**E**) Experimental optical absorption spectra at 0, 40, 50, 60, and 80% EtOH in H_2O (from blue to red: increasing % EtOH leads to decreasing average gap lengths). (**F**) Average fraction of light absorbed from 550 to 800 nm (dark purple) and wavelength of absorption band edge, λ_{edge} (pink). (**G**) Optical images of the disk-cube-sphere superlattice. Scale bar, 100 μm. (**H**) Optical absorption spectra are shown for five cycles between 0% (blue) and 80% (red) EtOH in H_2O.

by the initial band edge wavelength before tuning) of 19%. The tunability reported here exceeds that of stretchable substrates, which have exhibited wavelength tuning of up to 11% in the longer-wavelength infrared region (*30*) and is comparable to that achieved recently using temperature-responsive polymers (*31*). Importantly, all structural changes, and the changes they induce in optical properties, were reversible for at least five cycles between large and small gaps, with no appreciable changes to absorption spectra observed (Fig. 4H).

The ability to control the arrangement, spacing, and sequence of NPs within each architecture is critical to the realization of tunable broadband absorption. Indeed, superlattices with other sequences of disk, cube, and sphere Au NP architectures are predicted to exhibit very different optical responses with considerably reduced tunability (fig. S22). Beyond tunable absorption, the ability to make responsive plasmonic nanoarchitectures not yet achievable via other techniques should dramatically increase the diversity of structures and compositions that can now be explored by theorists and experimentalists to access new and useful optical properties. It should be possible to synthesize even more sophisticated architectures through the use of more intricate pore designs, and new DNA sequence designs should enable responsiveness to be extended to light and biological signals, in addition to chemical ones. Additionally, although we have only synthesized three-layer architectures here, the number of NP layers could in principle be increased by using deeper PMMA pores.

REFERENCES AND NOTES

1. C. A. Mirkin, R. L. Letsinger, R. C. Mucic, J. J. Storhoff, *Nature* **382**, 607–609 (1996).
2. D. Nykypanchuk, M. M. Maye, D. van der Lelie, O. Gang, *Nature* **451**, 549–552 (2008).
3. M. R. Jones, N. C. Seeman, C. A. Mirkin, *Science* **347**, 1260901 (2015).
4. Y. Wang *et al.*, *Nature* **491**, 51–55 (2012).
5. W. Liu *et al.*, *Science* **351**, 582–586 (2016).
6. W. B. Rogers, W. M. Shih, V. N. Manoharan, *Nat. Rev. Mater.* **1**, 16008 (2016).
7. M. N. O'Brien, H.-X. Lin, M. Girard, M. Olvera de la Cruz, C. A. Mirkin, *J. Am. Chem. Soc.* **138**, 14562–14565 (2016).
8. M. N. O'Brien, B. Radha, K. A. Brown, M. R. Jones, C. A. Mirkin, *Angew. Chem. Int. Ed.* **53**, 9532–9538 (2014).
9. Q.-Y. Lin *et al.*, *Nano Lett.* **15**, 4699–4703 (2015).
10. M. X. Wang *et al.*, *ACS Nano* **11**, 180–185 (2017).
11. J. Henzie, S. C. Andrews, X. Y. Ling, Z. Li, P. Yang, *Proc. Natl. Acad. Sci. U.S.A.* **110**, 6640–6645 (2013).
12. X. Liu *et al.*, *Adv. Mater.* **27**, 7314–7319 (2015).
13. V. Flauraud *et al.*, *Nat. Nanotechnol.* **12**, 73–80 (2017).
14. R. A. Hughes, E. Menumerov, S. Neretina, *Nanotechnology* **28**, 282002 (2017).
15. Materials and methods are available as supplementary materials.
16. R. J. Macfarlane *et al.*, *Science* **334**, 204–208 (2011).
17. V. A. Bloomfield, D. M. Crothers, I. Tinoco, *Nucleic Acids: Structures, Properties, and Functions* (University Science Books, Sausalito, CA, 2000).
18. A. A. Koshkin *et al.*, *Tetrahedron* **54**, 3607–3630 (1998).
19. R. Owczarzy, Y. You, C. L. Groth, A. V. Tataurov, *Biochemistry* **50**, 9352–9367 (2011).
20. J. Valentine *et al.*, *Nature* **455**, 376–379 (2008).
21. N. Liu *et al.*, *Nat. Mater.* **7**, 31–37 (2008).
22. M. A. Boles, M. Engel, D. V. Talapin, *Chem. Rev.* **116**, 11220–11289 (2016).
23. J. A. Mason *et al.*, *J. Am. Chem. Soc.* **138**, 8722–8725 (2016).
24. N. J. Halas, S. Lal, W.-S. Chang, S. Link, P. Nordlander, *Chem. Rev.* **111**, 3913–3961 (2011).
25. A. M. Urbas *et al.*, *J. Opt.* **18**, 093005 (2016).
26. N. I. Zheludev, E. Plum, *Nat. Nanotechnol.* **11**, 16–22 (2016).
27. Z. Qian, D. S. Ginger, *J. Am. Chem. Soc.* **139**, 5266–5276 (2017).
28. A. Moreau *et al.*, *Nature* **492**, 86–89 (2012).
29. G. M. Akselrod *et al.*, *Adv. Mater.* **27**, 8028–8034 (2015).
30. I. M. Pryce, K. Aydin, Y. A. Kelaita, R. M. Briggs, H. A. Atwater, *Nano Lett.* **10**, 4222–4227 (2010).
31. T. Ding *et al.*, *Proc. Natl. Acad. Sci. U.S.A.* **113**, 5503–5507 (2016).

ACKNOWLEDGMENTS

This material is based on work supported by the Center for Bio-Inspired Energy Science, an Energy Frontier Research Center funded by the U.S. Department of Energy, Office of Science, Basic Energy Sciences, under award DE-SC0000989 and the Air Force Office of Scientific Research under awards FA9550-12-1-0280, FA9550-14-1-0274, and FA9550-17-1-0348. Use of the Center for Nanoscale Materials, an Office of Science user facility at Argonne National Laboratory, and GISAXS experiments at beamline 12-ID-B at the Advanced Photon Source at Argonne National Laboratory were supported by the U.S. Department of Energy, Office of Science, Office of Basic Energy Sciences, under contract DE-AC02-06CH11357. This work made use of the Electron Probe Instrumentation Center (EPIC) facility of the Northwestern University Atomic and Nanoscale Characterization Experimental Center (NUANCE) at Northwestern University, which has received support from the Soft and Hybrid Nanotechnology Experimental (SHyNE) Resource (NSF NNCI-1542205); the Materials Research Science and Engineering Center program (NSF DMR-1121262) at the Materials Research Center; the International Institute for Nanotechnology (IIN); the Keck Foundation; and the State of Illinois, through the IIN. Q.-Y.L., Z.L., and M.R.J. gratefully acknowledge support from the Ryan Fellowship at Northwestern University, and M.N.O. gratefully acknowledges the National Science Foundation for a Graduate Research Fellowship. We thank C. Laramy and H. Lin for assistance with some nanoparticle syntheses. The authors declare no competing financial interests. All data are reported in the main text and the supplementary materials.

SUPPLEMENTARY MATERIALS

www.sciencemag.org/content/359/6376/669/suppl/DC1
Materials and Methods
Supplementary Text
Figs. S1 to S37
Table S1
References (*32*–*72*)

26 September 2017; accepted 26 December 2017
Published online 18 January 2018
10.1126/science.aaq0591

Building superlattices from individual nanoparticles via template-confined DNA-mediated assembly

Qing-Yuan Lin, Jarad A. Mason, Zhongyang Li, Wenjie Zhou, Matthew N. O'Brien, Keith A. Brown, Matthew R. Jones, Serkan Butun, Byeongdu Lee, Vinayak P. Dravid, Koray Aydin and Chad A. Mirkin

Science **359** (6376), 669-672.
DOI: 10.1126/science.aaq0591originally published online January 18, 2018

Programmed nanoparticle stacking

A polymer pore template can control the order of assembly of nanoparticles into well-defined stacks and create superlattices. Lin *et al.* used DNA strands on gold nanoparticles to control interparticle distance. The DNA strands contained modified adenines with more rigid ribose groups that formed stronger base pairs. The height of the stacks of three different types of gold nanoparticle could be changed with different solvents, which in turn changed their optical response.

Science, this issue p. 669